THE JOURNAL OF BIOLOGICAL CHEMISTRY Vol. 275, No. 33, Issue of August 18, pp. 25523–25532, 2000

Printed in U.S.A.

Poliovirus RNA-dependent RNA Polymerase ($3D^{pol}$)

STRUCTURAL, BIOCHEMICAL, AND BIOLOGICAL ANALYSIS OF CONSERVED STRUCTURAL MOTIFS A AND B*

Received for publication, March 29, 2000, and in revised form, May 10, 2000
Published, JBC Papers in Press, May 25, 2000, DOI 10.1074/jbc.M002671200

David W. Gohara‡§, Shane Crotty¶‖, Jamie J. Arnold‡, Joshua D. Yoder‡, Raul Andino¶, and Craig E. Cameron‡**

From the ‡Department of Biochemistry and Molecular Biology, Pennsylvania State University, University Park, Pennsylvania 16802 and ¶Department of Microbiology and Immunology, University of California, San Francisco, California 94143

We have constructed a structural model for poliovirus RNA-dependent RNA polymerase ($3D^{pol}$) in complex with a primer-template (sym/sub) and ATP. Residues found in conserved structural motifs A (Asp-238) and B (Asn-297) are involved in nucleotide selection. Asp-238 appears to couple binding of nucleotides with the correct sugar configuration to catalytic efficiency at the active site of the enzyme. Asn-297 is involved in selection of ribonucleoside triphosphates over 2′-dNTPs, a role mediated most likely via a hydrogen bond between the side chain of this residue and the 2′-OH of the ribonucleoside triphosphate. Substitutions at position 238 or 297 of $3D^{pol}$ produced derivatives exhibiting a range of catalytic efficiencies when assayed *in vitro* for poly(rU) polymerase activity or sym/sub elongation activity. A direct correlation existed between activity on sym/sub and biological phenotypes; a 2.5-fold reduction in polymerase elongation rate produced virus with a temperature-sensitive growth phenotype. These data permit us to propose a detailed, structural model for nucleotide selection by $3D^{pol}$, confirm the biological relevance of the sym/sub system, and provide additional evidence for kinetic coupling between RNA synthesis and subsequent steps in the virus life cycle.

All nucleic acid polymerases, with the exception of mammalian DNA polymerase β, have the same overall topology (1). As suggested first by Steitz in his description of the Klenow fragment of DNA polymerase I (KF)[1] (2), these enzymes resemble a cupped, right hand with fingers, palm, and thumb subdomains. The fingers and thumb subdomains contribute to substrate binding, especially to regions of primer and template remote from the catalytic center (3–7). The palm subdomain of all classes of polymerase contains structural elements necessary for phosphoryl transfer and binding to primer, template, and nucleotide (8–12). The overall structure and, to some extent, sequence of palm subdomains are also highly homologous. Thus, the functional similarity between the kinetic and chemical mechanism of nucleic acid polymerases is not surprising (13–17).

Nucleic acid polymerases are categorized based upon their specificity for template and nucleotide. Of course, specificity is a relative term, since it is quite dependent upon reaction conditions. At physiologically relevant values of pH and ionic strength and in the presence of Mg^{2+} ions, most DNA-dependent DNA polymerases prefer to utilize DNA templates and 2′-deoxyribonucleotides (2′-dNTPs) as substrates rather than RNA and ribonucleotides (rNTPs) (18). The converse is true for RNA-dependent RNA polymerases (RdRPs) (19, 20).

However, even under physiological conditions, exceptions to polymerase specificity have been noted, especially for primer and/or template utilization. For example, KF utilizes RNA templates (21), T7 DNA-dependent RNA polymerase (DdRP) utilizes RNA templates (22), and poliovirus RdRP utilizes DNA primers (20). Template preference becomes even more ambiguous when alternative divalent cations, such as Mn^{2+}, are employed (20). This "identity crisis" of polymerases regarding template utilization is not too surprising given the existence of enzymes like reverse transcriptases (RTs) that bridge both worlds (23). Moreover, the ease of polymerases to move from one template type to another was probably a driving force for the evolution of specific protein-nucleic acid and protein-protein interactions as an obligatory step for the initiation of transcription, replication, and repair (24).

In contrast to template selection, nucleotide selection is more stringent under physiological conditions. For example, T7 DdRP exhibits an 80-fold preference for rNTPs relative to 2′-dNTPs (25). KF exhibits a 10^3 to 10^6-fold preference for 2′-dNTPs (26–28). The reverse transcriptases from human immunodeficiency virus (HIV-1) and Moloney murine leukemia virus (MMLV) exhibit a 10^5-fold preference for 2′-dNTPs (29, 30). The use of Mn^{2+} as divalent cation permits all classes of polymerase to incorporate one or two nucleotides of the incorrect sugar configuration (31–36). However, processive incorporation of nucleotides of the incorrect sugar configuration is not tolerated (37, 38).

The molecular basis for nucleotide selection by polymerases has been a topic of considerable interest recently (39–43). This interest has resulted from the development of structural models for DNA-dependent DNA polymerases and a DdRP in complex with various substrates (*e.g.* primer, template, and/or nucleotide). These studies have uncovered interactions between the enzyme and nucleotide that may be important during the

* This work was supported in part by NCI, National Institutes of Health (NIH), Howard Temin Award CA75118 (to C. E. C.) and NIAID, NIH, Grants AI45818 (to C. E. C.) and AI40085 (to R. A.). The costs of publication of this article were defrayed in part by the payment of page charges. This article must therefore be hereby marked "*advertisement*" in accordance with 18 U.S.C. Section 1734 solely to indicate this fact.

§ Predoctoral fellow supported by National Science Foundation Research Training Grant DBI-902232.

‖ Howard Hughes Medical Institute predoctoral fellow.

** To whom correspondence should be addressed. Tel.: 814-863-8705; Fax: 814-863-7024; E-mail: cec9@psu.edu.

[1] The abbreviations used are: KF, Klenow fragment; rNTP, ribonucleoside triphosphate; HIV-1, human immunodeficiency virus-1; RT, reverse transcriptase; MMLV, Moloney murine leukemia virus; RdRP, RNA-dependent RNA polymerase; DdRP, DNA-dependent RNA polymerase; PCR, polymerase chain reaction.

selection process (5–9). Construction and characterization of site-directed mutants of KF, HIV-1 RT, and MMLV RT have confirmed the structural predictions by altering the 2′-dNTP/rNTP preference of these enzymes. The 2′-dNTP-utilizing enzymes use a steric gating mechanism to decrease the affinity of the enzyme for rNTPs (27, 28, 40). The steric gate is formed, in part, by a residue found in structural motif A (motif designations are as defined by Hansen *et al.* (1)) of the palm subdomain (KF Glu-710, HIV-1 RT Tyr-115, MMLV RT Phe-155). Structural motif B of the palm subdomain may also participate in this process (43).

The mechanism employed by rNTP-utilizing enzymes is not fully understood. A steric gating mechanism has been proposed for T7 DdRP. Succinctly, it has been suggested that a water molecule bound to Tyr-639, a residue that occludes the nucleotide-binding pocket, is displaced as a consequence of rNTP binding. Displacement of this water molecule results in movement of Tyr-639 out of the pocket, thereby permitting productive rNTP binding. The absence of a 2′-OH would not permit induction of this conformational transition, thereby creating a steric block to productive binding of 2′-dNTPs (25, 44). Although this model is based upon steady-state kinetic analysis of T7 RNA polymerase derivatives, a water molecule and movement of Tyr-639 have been observed crystallographically (45, 46).

An alternative model has been proposed recently for rNTP selection by T7 DdRP based solely upon structural observations. Selection for rNTP binding appears to be mediated by a hydrogen-bonding network consisting of the 2′-OH and side chains of the enzyme (His-784 and Tyr-639). Such a network is more consistent with the 80-fold preference of this enzyme for rNTPs (25, 47). An 80-fold difference in specificity corresponds to a free energy difference of approximately 3 kcal/mol, a reasonable value for one or two hydrogen bonds (67). Moreover, as discussed above, steric mechanisms yield specificity differences that are, on average, 4000-fold greater than that observed for this enzyme. Aspects of these two models are mutually exclusive. Analysis of His-784 derivatives under conditions in which 2′-dNTP incorporation by the wild-type enzyme is observed should help to distinguish between these two models (45).

Currently, information regarding the mechanism of nucleotide selection by the RdRP is not available. Our previous work has shown that the RdRP from poliovirus utilizes rNTPs at least 121-fold more efficiently than 2′-dNTPs (48). This value is similar to that determined for T7 DdRP. In addition, Hansen *et al*. have predicted the use of a hydrogen-bonding network to select for rNTP binding based upon the unliganded structure of this enzyme (1). In this report, we have used the structure for the ternary complex of HIV-1 RT to develop a model for the ternary complex of poliovirus RNA polymerase. In addition, we use biochemical and biological analysis of site-directed mutants of 3D^{pol} to test predictions of this model. This analysis demonstrates a role for conserved structural motifs A and B in 2′-dNTP/rNTP selection by the RdRP. In addition, we provide additional support for the biological relevance of the primer-template (sym/sub) system developed to study the RdRP from poliovirus *in vitro* (48).

EXPERIMENTAL PROCEDURES

Materials—[α-^{32}P]UTP (>6,000 Ci/mmol) was from NEN Life Science Products; [γ-^{32}P]ATP (>7,000 Ci/mmol) was from ICN; nucleoside 5′-triphosphates (ultrapure solutions) were from Amersham Pharmacia Biotech, Inc.; all DNA oligonucleotides and T4 DNA ligase were from Life Technologies, Inc.; all RNA oligonucleotides were from Dharmacon Research, Inc. (Boulder, CO); restriction enzymes, T4 polynucleotide kinase, and Deep Vent DNA polymerase were from New England Biolabs, Inc.; polyethyleneimine-cellulose TLC plates were from EM Science; and 2.5-cm DE81 filter paper discs were from Whatman. All other reagents were of the highest grade available from Sigma or Fisher.

Construction of the 3D^{pol} Ternary Complex Model—The coordinates for the HIV-1 RT ternary complex (1rtd) and 3D^{pol} (1rdr) are available from the Research Collaboratory for Structural Bioinformatics. Superpositioning of the two structures was performed using lsqkab from the CCP4 suite of programs (49). Structural alignments were initially performed using the thumb and palm subdomains. Final superpositioning of the two structures was confined to structural motifs A (3D^{pol} residues 233–240), B (287–302), C (324–331), and E (368–380). The final positions of C-α atoms in the four structural motifs had a root mean square deviation ranging from 0.9 to 1.8 Å.

3D^{pol} residues were inserted into the structurally analogous positions of HIV-1 RT using the program O (50). Residues having the same identity in both structures were not altered from those observed in the HIV-1 RT structure. Amino acids unique to 3D^{pol} were manually set in position based on their orientation in the unliganded 3D^{pol} structure. In some instances, the side chains were adjusted to eliminate steric contact with neighboring residues. 2′-OHs were inserted into both the primer and template strands of the nucleic acid within the polymerase active site as well as the incoming nucleotide. Bond angles for the 2′-OHs were adopted from various RNA structures determined using NMR and x-ray crystallography obtained from the Research Collaboratory for Structural Bioinformatics. Within the vicinity of the active site, DNA in the HIV-1 RT structure adopts an A-form conformation causing the sugar pucker to switch from C2′-endo to C3′-endo; hence, modification of the sugar geometry was not necessary. Nucleotide bases of the RNA were modified to correspond to that of sym/sub (48), 5′-GCAUGGGCCC-3′, and the incoming nucleotide was modified to ATP, the first nucleotide incorporated into sym/sub. Two additional regions (comprising residues 163–202) were modeled into the structure based on a partial structural and sequence alignment. Region I, residues 175–202, was identified by superpositioning of the 3D^{pol} and HIV-1 RT structures and consists of an extended α-helix that runs underneath the 3′-end of the template strand. Region II comprises residues 163–174 (which are absent from the 3D^{pol} structure), which represent the active site side of the fingers subdomain.

Energy minimizations were performed on the entire structure, comprising both modified and unmodified regions, using the program CNS SOLVE (51). Initial attempts at energy minimization were performed on the modified region of the structure only; however, upon completion of the first cycle, gross distortions of the molecule were observed. The modified region was reinserted into the entire HIV-1 RT structure, and energy minimizations were repeated. The additional structure eliminated distortions in the molecule, allowing the protein side chains to relax into positions void of unfavorable, steric contact. Iterative cycles of minimization, a total of 10, were performed using the constant temperature algorithm. The final settings for the energy minimization follow. The Cartesian (restrained) molecular dynamics algorithm was utilized at a constant temperature (298 K) using the coupled temperature control method (52). 10,000 molecular dynamics steps were performed at 0.0005-ps intervals. The dielectric was set to 1 (the default value), and the number of trials utilizing different initial velocities was set to 1. The output files from each cycle were superimposed to observe side chain and nucleic acid motions, which were most apparent for side chains and nucleotides not involved in protein or nucleic acid interactions. Upon completion of the final cycle of minimization, the modified region was removed from the structure, and side chain geometry was checked using the program PROCHECK (53). Finally, the modified regions of the HIV-1 RT structure, as well as nucleic acid, nucleotide, and Mg^{2+} ions were removed from the file and used to generate a new Protein Data Bank file (3DRTSS).

Construction, Expression, and Purification of 3D^{pol} Derivatives—Mutations were introduced into a modified 3D^{pol}-coding sequence by using overlap-extension PCR (54) and expressed in *Escherichia coli* by using a ubiquitin fusion system. The ubiquitin fusion system, PCR conditions, and modified gene have been described previously (55). The D238F clone was engineered such that it contained a silent *Nhe*I site. The sequence of the forward oligonucleotide is 5′-GAC TAC ACA GGG TAT TTC **GCT AGC** CTC AGC CCT-3′; the codon changing Asp to Phe is underlined, and the *Nhe*I site is in boldface type. A wild-type reverse oligonucleotide was employed (oligonucleotide 10, Table I). Briefly, two separate PCR reactions were performed: one reaction with the pET-Ub-SacII for oligonucleotide and the Asp-238 WT rev; the other with D238 wild-type rev for and pET-3D-BamHI rev. Both reactions employed pET26b-Ub-3D (55) as template. Products were purified by agarose gel electrophoresis and used as the template in the next round of PCR with a 1:10 molar ratio of the wild-type:D238F-modified fragments. The *Afl*II for and *Avr*II reverse oligonucleotides were used as the sole primers for

TABLE I
Oligonucleotides used in this study

Oligonucleotide no.	Oligonucleotide name	Sequence
1	pET-Ub-SacII for	5′-GCG GAA TTC CCG CGG TGG AGG TGA AAT CCA GTG G-3′
2	pET-Ub-BamH I rev	5′-GCG TCT AGA GGA TCC ACC GCG GAG-3′
3	3D AflII for	5′-AAA AAC GAT CCC AGG CTT AAG ACA GAC TTT-3′
4	3D AvrII rev	5′-CCT GAG TGT TCC TAG GAT CTT TAG T-3′
5	D238A for	5′-GAC TAC ACA GGG TAT GCT GCA TCT CTC AGC CCT-3′
6	D238E for	5′-GAC TAC ACA GGG TAT GAA GCA TCT CTC AGC CCT-3′
7	D238F Nhe for	5′-GAC TAC ACA GGG TAT TTC GCA TCT CTC AGC CCT-3′
8	D238N for	5′-GAC TAC ACA GGG TAT AAC GCA TCT CTC AGC CCT-3′
9	D238V for	5′-GAC TAC ACA GGG TAT GTT GCA TCT CTC AGC CCT-3′
10	D238 wild-type rev	5′-AGG GCT GAG AGA TGC ATC ATA CCC TGT GTA GTC-3′
11	N297A for	5′-GGC ACT TCA ATT TTT GCT TCA ATG ATT AAC AAC-3′
12	N297D for	5′-GGC ACT TCA ATT TTT GAC TCA ATG ATT AAC AAC-3′
13	N297F for	5′-GGC ACT TCA ATT TTT TTC TCA ATG ATT AAC AAC-3′
14	N297Q for	5′-GGC ACT TCA ATT TTT CAG TCA ATG ATT AAC AAC-3′
15	N297V for	5′-GGC ACT TCA ATT TTT GTT TCA ATG ATT AAC AAC-3′
16	N297 wild-type rev	5′-GTT GTT AAT CAT TGA GTT AAA AAT TGA AGT GTT-3′
17	pUC18BslII top	5′-GAT CCA GAT CTA GTA CTG-3′
18	pUC18BglII bot	5′-AAT TCA GTA CTA GAT CTG-3′
19	pMoEcoRI rev	5′-GAA TTA AAT CAT CGA TGA ATT CGG GCC C-3′
20	pMoBglII for	5′-GAA GTG GAG ATC TTG GAT GCC AAA GCG-3′
21	N-term-Ub	5′-ACG CTG TCT GAT TAC AAC-3′
22	pET-3D-rev	5′-TTG GCT TGA CTC ATT TTA GTA AGG ATC CGA ATT CCG C-3′

this cycle of PCR. Product was purified, digested with *Avr*II and *Afl*II, and ligated into pET26b-Ub-3D that had been digested with the same restriction enzymes. Plasmids were screened for the presence of the *Nhe*I site. The remaining mutant 3D^{pol} genes were constructed by using PCR as described above and subcloned into the D238F vector between the *Afl*II and *Avr*II restriction sites and screened for the loss of the *Nhe*I site. Mutations were confirmed by DNA sequencing (Nucleic Acid Facility, Pennsylvania State University).

3D^{pol} derivatives were expressed and purified as described previously (55) with the following modifications. 100-ml cultures were lysed by using a French press, nucleic acid was removed by precipitation with polyethyleneimine, and supernatants were clarified by ultracentrifugation (55). 3D^{pol} was precipitated by the addition of solid ammonium sulfate to 40% saturation. Recovered pellets were suspended and passed over a 3-ml phosphocellulose column. Bound protein was eluted from the phosphocellulose column by using ⅙ column volume (500 μl) of 50 mM HEPES, pH 7.5, 10 mM dithiothreitol, 20% glycerol, 0.1% Nonidet P-40, and 200 mM NaCl. The proteins were >90% pure based upon SDS-polyacrylamide gel electrophoresis analysis. Two of the derivatives (D238A and N297A) were purified using the complete purification procedure (55) to >95% purity. The N297F derivative was not soluble when induced in *E. coli* at 25 °C. The concentration of all 3D^{pol} derivatives was determined by absorbance at 280 nm using a calculated extinction coefficient of 71,480 M^{-1} cm^{-1} (56). The concentration of enzyme stocks prepared by using the abbreviated procedure ranged from 43 to 51 μM.

Purity of [α-^{32}P]UTP—[α-^{32}P]UTP was diluted to 0.1 μCi/μl in distilled deionized H_2O, and 1 μl was spotted in triplicate onto TLC plates. TLC plates were developed in 0.3 M potassium phosphate, pH 7.0, dried, and exposed to a PhosphorImager screen (Molecular Dynamics, Inc., Sunnyvale, CA). Imaging and quantitation were performed by using the ImageQuant software from Molecular Dynamics. The purity was used to correct the specific activity of UTP in reactions in order to calculate accurate concentrations of product.

Poly(rU) Polymerase Activity Assays—Reactions contained 50 mM HEPES, pH 7.5, 10 mM 2-mercaptoethanol, 5 mM $MgCl_2$ or $MnCl_2$, 60 μM $ZnCl_2$, 500 μM UTP, 0.4 μCi/μl [α^{32}-P]UTP, 1.8 μM dT_{15}/2 μM rA_{30} primer-template, and 3D^{pol}. Reactions were carried out in a total volume of 25 μl with 250 ng of enzyme at 30 °C for 5 min. Reactions were quenched by the addition of 5 μl of 0.5 M EDTA. 10 μl of the quenched reaction was spotted onto DE81 filter paper discs and dried completely. The discs were washed three times for 10 min in 250 ml of 5% dibasic sodium phosphate and rinsed in absolute ethanol. Bound radioactivity was quantitated by liquid scintillation counting in 5 ml of EcoScint scintillation fluid (National Diagnostics).

5′-^{32}P Labeling of Oligonucleotides—RNA oligonucleotides were end-labeled using [γ-^{32}P]ATP and T4 polynucleotide kinase essentially as specified by the manufacturer. Reactions typically contained 11 μM [γ-^{32}P]ATP, 10 μM RNA oligonucleotide, and 0.4 units/μl T4 polynucleotide kinase. Unincorporated nucleotide was removed by passing the sample over two consecutive 1-ml Sephadex G-25 (Sigma) spun columns.

Kinetics of Single Ribo- and Deoxyribonucleotide Incorporation—Rates of nucleotide incorporation were determined using a synthetic RNA oligonucleotide primer-template (sym/sub) (48). Reactions were performed either on the bench top or in an RQF-3 rapid quenching/mixing device (KinTek Corp., Austin, TX) (57). Enzyme-nucleic acid complexes were preformed by incubating 2 μM end-labeled sym/sub and 2 μM enzyme for 90–200 s at 30 °C in 50 mM HEPES, pH 7.5, 5 mM $MgCl_2$ or $MnCl_2$, 10 mM β-mercaptoethanol, 60 μM $ZnCl_2$. Reactions were initiated by the addition of an equal volume of nucleotide in the above buffer. At indicated times, the reaction was quenched by the addition of 0.5 M EDTA to a final concentration of 0.3 M.

Denaturing Polyacrylamide Gel Electrophoresis—10 μl of the quenched reaction was added to 10 μl of loading buffer: 90% formamide, 50 mM Tris borate, 0.025% bromphenol blue, 0.025% xylene cyanol. Samples were heated to 70 °C for 2–5 min prior to loading 5 μl on a 23% polyacrylamide, 1.5% bisacrylamide, 7 M urea gel. Electrophoresis was performed in 1× TBE (89 mM Tris, pH 8.0, 10 mM boric acid, 2 mM EDTA) at 75 watts. Gels were visualized by using a PhosphorImager (Molecular Dynamics) and quantitated by using ImageQuant software (Molecular Dynamics).

Data Analysis—Data were plotted using the program Kaleidagraph (Synergy Software, Reading, PA). The rate of nucleotide incorporation (k_{obs}) was determined by fitting the data to a single exponential, $k_{obs} = A \times \exp^{-kt} + C$, where A represents the maximum amplitude, k represents the observed rate of nucleotide incorporation, and t represents time. The maximum rate of nucleotide incorporation (k_{pol}) and the apparent binding constant (K_d) were determined by replot of k_{obs} *versus* [nucleotide] and fit to the following equation: $k_{obs} = ((k_{pol} \times [\text{nucleotide}])/(K_d + [\text{nucleotide}]))$.

Construction of Mutated Viral cDNA Clones (pMo-3D)—Cloning of mutated 3D^{pol}-coding sequence into the plasmid containing the full-length cDNA of poliovirus (pMoRA, also known as pXpA-rib$^+$polyAlong (58)) required subcloning into an intermediate pUC plasmid due to conflicting restriction sites in the pMoRA plasmid. *Bgl*II and *Sca*I restriction sites were introduced into a pUC18 plasmid by insertion of a synthetic linker between the *Bam*HI and *Eco*RI sites of this vector. The linker oligonucleotides (oligonucleotides 17 and 18, Table I) were annealed prior to ligation. *Sca*I was used to screen clones for the presence of the linker. The cDNA encoding the 3CD region of the wild-type Mahoney strain of poliovirus was PCR-amplified from pMoRA using the DNA oligonucleotides: pMoEcoRI rev (oligonucleotide 19, Table I) and pMoBglII for (oligonucleotide 20, Table I). The PCR product was ligated into the modified pUC18 vector using the *Bgl*II and *Eco*RI restriction sites. The entire insert was sequenced, and this construct was designated pUC-3CD.

Each mutated 3D^{pol}-coding sequence was PCR-amplified from the appropriate pET26b-Ub-3D plasmid using the DNA oligonucleotides: N-Term-Ub (oligonucleotide 21, Table I) and pET-3D-rev (oligonucleotide 22, Table I). The PCR product was digested with *Bst*BI and *Mfe*I

and ligated into appropriately digested pUC-3CD. The mutated viral cDNA clones were constructed by subcloning the *Bgl*II–*Eco*RI fragment from pUC-3CD into pMoRA. These final constructs were sequenced from the *Bst*BI site through the *Mfe*I site.

Construction of Mutated Replicons (pRLuc-3D)—The pRLuc-3D clones were constructed by subcloning the *Bgl*II–*Apa*I fragment from pMo-3D constructs containing the mutated 3D genes into pRLucRA (also known as pRLuc31-rib$^+$polyAlong) (58, 59).

Cells and Transfections—HeLa S3 (ATCC stock plus 10–30 passages) were propagated in DMEM/F-12 (Life Technologies, Inc.) supplemented with 10% fetal calf serum (Life Technologies), always keeping the cultures between 20 and 80% confluence. For infectious center assays, viral RNA was produced by *in vitro* transcription of linearized plasmids (pMoRA wild-type plasmid or the appropriate pMo-3D^{pol} derivative) using T7 RNA polymerase as described (60). 10 μg of each viral RNA transcript was electroporated into 1.2×10^6 HeLa cells in 400 μl in a 0.2-cm cuvette using electroporation settings of 950 microfarads, 24 ohms, and 130 V on a BTX electroporator, giving an average pulse length of 5 ms. Electroporated cells were separately diluted (10-fold) in phosphate-buffered saline, and 100 μl of appropriate dilutions (10^{-1} to 10^{-5}) was plated on 2×10^5 HeLa cells (prepared 1 day in advance) in six-well dishes (a total volume of 0.5 ml). The remainder of the undiluted electroporated cells were also plated. Cells were allowed to adsorb to the plate for 1–2 h at 37 °C or 32 °C, and then the medium/phosphate-buffered saline was aspirated, and the cells were overlaid with 3 ml of a mixture of 1× DMEM/F-12 plus 10% fetal calf serum and 1% agar. Infectious center assays were then incubated at 37 °C or 32 °C for 2 days (wild type at 37 °C), 3 days (wild-type at 32 °C), or 7 days (3D^{pol} mutant viruses). Plates were stained with the vital dye crystal violet, and viral plaques were counted.

Replicon transfections were performed using polioLuc RNA transcribed from the plasmid pRLucRA (58) or the pRLuc-3D derivatives detailed above using electroporation conditions described above. 1×10^5 cells were added per well to six-well dishes in prewarmed (37 or 32 °C) DMEM/F-12 plus 10% fetal calf serum medium. Cells were harvested at various times by centrifugation at $14,000 \times g$ for 2 min in an Eppendorf microcentrifuge and lysed in 100 μl of 1× cell culture lysis reagent (Promega, Madison, WI) on ice for 2 min, and cellular debris and nuclei were removed by centrifugation at $14,000 \times g$ for 1 min. Lysates were left on ice at 4 °C until all time points were collected. Lysates were diluted 1:100 in H_2O and assayed for luciferase activity after mixing 10 μl of lysate with 10 μl of luciferase assay substrate (Promega) by using an OptocompI luminometer (MGM).

RESULTS AND DISCUSSION

Model for the Ternary Complex of 3D^{pol}—As a first step toward elucidating the structure-function relationships of the RNA-dependent RNA polymerase from poliovirus (3D^{pol}), we constructed a model of a complex comprising the enzyme, primer-template, and nucleotide. The final structural model consists of structural motifs A, B, C, and E, nucleic acid primer-template, incoming nucleotide, and Mg^{2+} ions. In addition, an extended α-helix that supports the template strand, the loop leading into motif B, and the active site portion of the fingers subdomain were constructed. The last two elements were missing in the 3D^{pol} structure (1) (Fig. 1*A*).

This model contains features that offer insight into the roles of conserved residues of the RdRP. RdRPs contain a signature GDD motif (structural motif C) consisting of a strictly conserved glycine (Gly^{327}) as well as an aspartic acid (Asp^{328}). A structurally analogous aspartic acid has been observed at this position in all nucleic acid polymerases studied to date; however, the role of the conserved glycine in the RdRP remains unclear. Comparison of the 3D^{pol} ternary complex model with the HIV-1 RT ternary complex structure offers insight into the functional significance of a glycine at this position. In the 3D^{pol} model, the presence of a bulky side chain, such as methionine, would clash with the 2′-OH on the primer strand (Fig. 1*B*).

While the fingers subdomain is not present in the unliganded structure for 3D^{pol}, superpositioning of the two structures results in the alignment of an extended α-helix (3D^{pol} residues 183–202) with a β-strand (HIV-1 RT residues 78–94). In HIV-1 RT, this β-strand leads into a segment of the enzyme that forms the active site side of the fingers subdomain, referred to here as the β flap (β3-β4). Sequence homology permitted the assignment of 3D^{pol} residues 163–174, which correspond to the β flap of HIV-1 RT. Recently, the complete structure for the RdRP from hepatitis C virus (HCV NS5B) was determined (10, 11). Structural comparisons of the fingers region of NS5B and HIV-1 RT identified a new structural motif (motif F) (11). The assignment of residues 163–174 of 3D^{pol} to motif F is in agreement with structural information now available for NS5B. Conserved, basic residues located in motif F of 3D^{pol}, Lys-167 and Arg-174, are predicted to make contact with the phosphate moiety of the incoming nucleotide, consistent with interactions observed in the HIV-1 RT ternary complex structure (Fig. 1*B*) (7).

Nucleotide cross-linking studies with 3D^{pol} have suggested that another conserved residue, Lys-66, is required for activity both *in vitro* and *in vivo* and may be in direct contact with the incoming nucleotide (61). While the Lys-66 side chain is disordered in the 3D^{pol} structure, structural and sequence homology to NS5B would place this residue at the border of the NTP channel leading to the polymerase active site. Modeling of nucleic acid and nucleotide into the NS5B structure places the analogous residue to Lys-66, Lys-56, approximately 3.0 Å away from the incoming nucleoside triphosphate (data not shown). Lys-66 may therefore be required to direct the incoming nucleotide into the active site and/or stabilize the tripolyphosphate moiety by making contact with oxygens on the γ-phosphate.

DNA polymerases most likely select for 2′-dNTPs by using a steric gating mechanism that excludes the bulky 2′-OH present on rNTPs. Residues in conserved structural motifs A and B appear to be important mediators of the selection against rNTP binding (27, 29, 62). Mutation of Glu-710 (KF) and Phe-155 (MMLV RT) to alanine and valine, respectively, produces derivatives that are less likely to discriminate against a rNTP when compared with the wild-type enzyme (27, 30). While these enzymes are capable of incorporating a rNTP more efficiently than their wild-type counterparts, multiple cycles of rNTP incorporation may be prohibited by the steric interactions with residues on motif C (see above).

Based upon structural homology to residues in DNA polymerases, it was put forward that Asp-238 and Asn-297 of 3D^{pol} are important for nucleotide selection at the 2′-position of the rNTP (1). Specifically, it was suggested that selection for the presence of a 2′-OH is mediated by a hydrogen-bonding network; Asp-238 is positioned in the active site by Asn-297 to hydrogen-bond to the 2′-OH of the incoming rNTP (1) (Fig. 2*A*). In contrast to the unliganded structure, the final model for the ternary complex of 3D^{pol} shows Asp-238 hydrogen bonding to a highly conserved threonine (Thr-293), while Asn-297 is interacting with the 2′-OH of the incoming nucleotide (Fig. 2*B*). In addition, an interaction between the Asp-238 backbone amide and the 3′-OH is also predicted (Fig. 2*B*); a similar interaction has been observed in the RT ternary complex (7). This hydrogen bond will not form based upon the conformation of this residue in the unliganded structure (Fig. 2*A*) (1). Given the difference between the unliganded structure and the model (Fig. 2*C*), substitutions were made at both positions to determine the functional significance of a hydrogen bond between these two residues. Furthermore, because both residues are strictly conserved in the supergroup I and III RdRPs and highly conserved in supergroup II polymerases (63), functional analysis of these amino acids is important to begin to understand the roles of these conserved side chains which line the nucleotide-binding pocket.

Rationale for Mutations—In order to test the functional significance of the hydrogen-bonding interaction between Asp-238

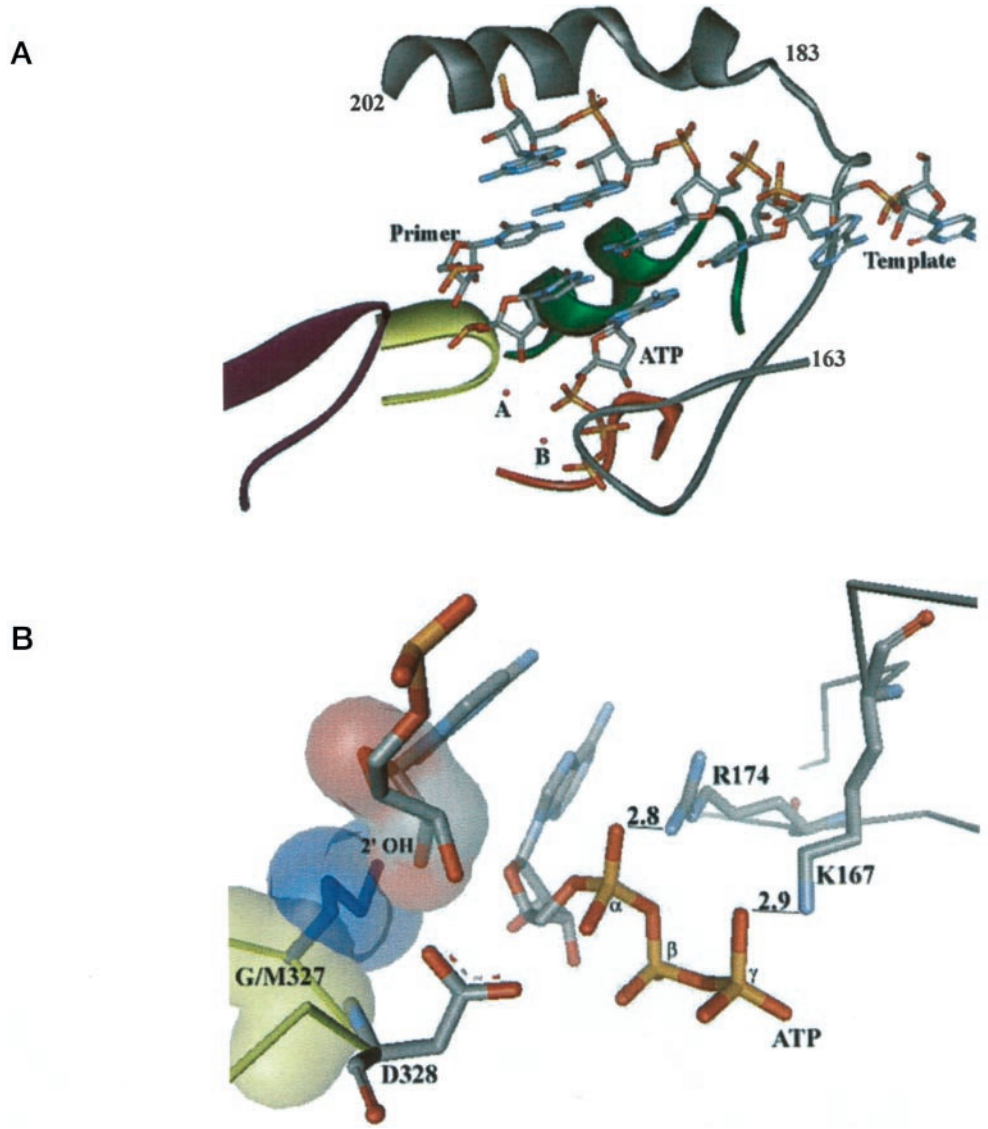

FIG. 1. **Structural model for the ternary complex of 3D^pol.** *A*, structural model for 3D^pol complex with RNA primer-template (sym/sub), ATP, and Mg^{2+}. Model construction is described under "Experimental Procedures." Structural motifs are color-coded according to Hansen *et al.* (1) as follows: *red*, motif A (residues 233–240); *green*, motif B (287–302); *yellow*, motif C (324–331); *dark purple*, motif E (368–380). The proposed active site portion of the fingers subdomain (motif F, 163–182) and the α-helical extension (183–202) are colored *gray*. Primer, template, and ATP are shown as *stick models*, and color coding is as follows: *red*, oxygen; *blue*, nitrogen; *orange*, phosphorus; *gray*, carbon. Metal ions A and B are shown as *magenta spheres*. For clarity, only the last two nucleotides on the 3′-end of the primer are shown. *B*, proposed function of a glycine residue in the "GDD" motif (motif C) and conserved residues in motif F. Van der Waal's projection of the strictly conserved glycine (*yellow surface*) of motif C (*yellow strand*) at the 3′-end of the primer. Met-184 of HIV-1 RT has been superimposed into the model (*blue stick* and *surface*). The presence of the bulky side chain of methionine would sterically occlude the 2′-OH at the 3′-end of the primer strand. Asp-328 and the 3′-OH of the primer strand help to coordinate metal ion at site A (see Fig. 1*A*). The 3′-OH is positioned for an in-line attack of the α-phosphorus of the incoming nucleotide. Lys-167 and Arg-174 on motif F (*gray strand*) are shown hydrogen-bonding to oxygens of the γ- and α-phosphates of the incoming nucleotide. The *numbers* shown are hydrogen bond distances (in Ångstroms). All structural diagrams were generated using the program WebLabViewer (Molecular Simulations Inc., San Diego, CA).

and Asn-297, a series of mutations were introduced into 3D^pol-coding sequence. These mutations changed Asp-238 to alanine, asparagine, glutamic acid, phenylalanine, or valine or changed Asn-297 to alanine, aspartic acid, glutamine, phenylalanine, or valine. Alanines were substituted at either position (D238A or N297A) such that a hydrogen bond between Asp-238 and Asn-297 would be disrupted. The structurally analogous residues of the DNA-dependent DNA polymerases (D238E or N297Q) and reverse transcriptases (D238F or N297F) were substituted. If a steric interaction and not a hydrogen bond is important for activity, then substitution of valine may be sufficient for 3D^pol activity (D238V or N297V). Finally, substitution of the pairing partner of either two residues (D238N or N297D) may be sufficient to retain the hydrogen bond and have little effect on activity. If a hydrogen bond between Asp-238 and Asn-297 is required for rNTP selection, then substitutions at either position that would disrupt hydrogen bonding should result in 3D^pol derivatives that have equivalent phenotypes.

Activity on Homopolymeric Primer-Templates—In order to assess the effects of substitutions at positions 238 and 297 on polymerase activity, we evaluated the $(dT)_{15}$-primed poly(rU) polymerase activity of each 3D^pol derivative by using a dT_{15}-rA_{30} primer-template (21). If a hydrogen bond between Asp-238 and Asn-297 is required for polymerase function, then substitutions at either position should equally impair polymerase activity. However, an equivalent phenotype was not observed. Substitutions at position 238 almost completely abolished activity (1–7% of wild type), while substitutions at position 297

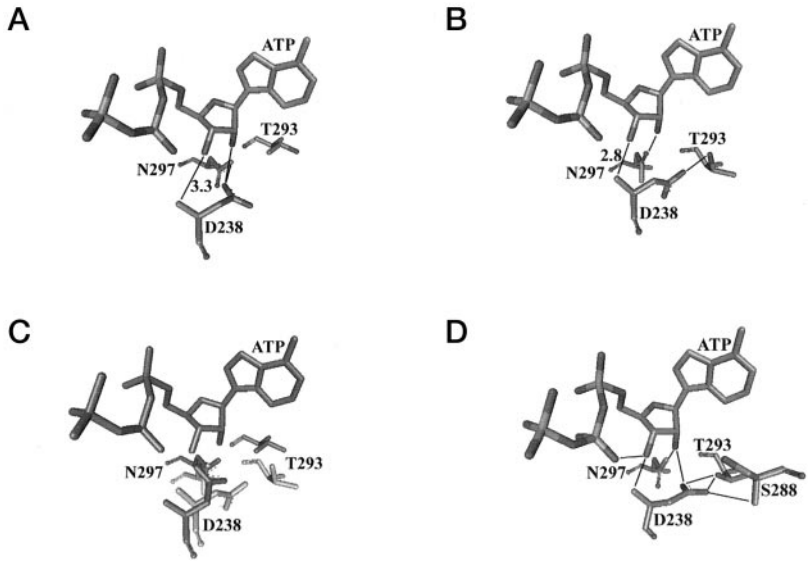

FIG. 2. **Analysis of the unliganded structure and ternary complex model of 3D^{pol}.** *A*, Asp-238 (motif A) and Asn-297 (motif B) are shown interacting at a distance of 3.0 Å, based on a modified version (see below) of the coordinate file for the unliganded structure of 3D^{pol} (1); Thr-293 (motif B) is approximately 4.5 Å away from Asp-238. Superpositioning of the unliganded 3D^{pol} structure onto the ternary complex structure of HIV-1 RT shows steric clash between Asp-238 and the 2′- and 3′-OHs of the nucleotide. To avoid unfavorable steric contact, either the side chain of Asp-238 must move relative to the incoming nucleotide or the position of the nucleotide itself must be altered. However, the position of the nucleotide in the active site is constrained by hydrogen bonds between the phosphate moiety and the protein backbone, the position of the 3′-OH of the primer relative to the α-phosphate, and hydrogen bonding/stacking interactions of the base. A similar motion of Asp-225 (Asp-238 homologue) in NS5B is also required given the above constraints. *B*, the ternary complex model indicates that Asp-238 is a distance of 2.8 Å from Thr-293, while Asn-297 is within hydrogen bonding distance (3.3 Å) of the 2′-OH of the incoming nucleotide (ATP). The 3′-OH and an oxygen of the β-phosphate are within hydrogen bonding distance. *C*, superposition of the unliganded 3D^{pol} structure (*dark gray*) with the ternary complex model (*light gray*) predicts a conformational change of the enzyme after rNTP binding. *D*, proposed model for rNTP selection. Asn-297 hydrogen bonds to the 2′-OH of the incoming rNTP. Asp-238 is within hydrogen bonding distance of the 2′-OH of the incoming nucleotide in a conformation that is stabilized by hydrogen bonds to Thr-293 as well as the backbone amide of Ser-288. The 3′-OH of the incoming nucleotide makes contact with the backbone amide of Asp-238 and is within hydrogen bonding distance of the oxygen on the β-phosphate, thus providing a link between the nucleotide-binding pocket and the catalytic center of 3D^{pol}.

had only moderate effects (20–80% of wild type) (Table II).

Derivatives containing substitutions that mimic the nucleotide-binding site of DNA polymerases (D238F, D238E, and N297Q) were analyzed for poly(dT) polymerase activity. Incorporation of dTMP was not observed with any of the derivatives by using this assay (data not shown). It was possible that incorporation of dNMPs required "proper" positioning of the enzyme on the primer-template. In the previous experiments, a DNA primer was employed. Perhaps an RNA primer could support dNMP incorporation. To test this possibility, incorporation of ribonucleoside monophosphates and dNMPs was evaluated by using an $(rU)_{15}$ primer. Again, dNMP incorporation was not observed (data not shown).

Changing Asp-225 of NS5B (Asp-238 homologue) to glycine or asparagine resulted in a complete loss of activity (64). Changing Asp-240 of encephalomyocarditis virus 3D^{pol} to glutamic acid produced an enzyme with a 33-fold reduction in activity (65). However, based upon poly(rU) polymerase activity, substitutions at the Asn-297 equivalent of 3D^{pol} resulted in either a complete loss of activity or significantly reduced activity (6% of wild-type) for NS5B and encephalomyocarditis virus 3D^{pol}, respectively. While these results are in partial agreement with our observations, alternative substrates were not available to evaluate these substitutions further, making interpretation of these differences difficult.

It is possible that substitutions at Asp-238 may have resulted in large rearrangements of the nucleotide-binding pocket. To test the catalytic competence of the 3D^{pol} derivatives, Mn^{2+} was substituted for Mg^{2+} in the poly(rU) polymerase assays, because Mn^{2+} is known to stimulate wild-type 3D^{pol} (20). All of the derivatives could be stimulated in the presence of Mn^{2+}, albeit to various degrees (Table II). Substitutions at Asn-297 could be stimulated to wild-type levels or greater than wild-type levels observed in Mg^{2+}. For three of the five substitutions at Asp-238, approximately 75% of the wild-type activity could be restored by using Mn^{2+}. Two of the derivatives (D238F and D238V) showed only a slight increase in poly(rU) polymerase activity, suggesting that the presence of larger hydrophobic residues at this position may, in fact, distort the nucleotide-binding pocket. Taken together, these results suggest that in most instances major structural rearrangements do not occur when substitutions are made at positions 238 and 297 and that a hydrogen bond between Asp-238 and Asn-297 is not absolutely required for polymerase activity.

TABLE II
Poly(rU) polymerase activity of wild-type 3D^{pol} and 3D^{pol} derivatives determined by using dT_{15}/rA_{30}

Specific activities were determined as described under "Experimental Procedures."

Enzyme	Specific activity[a]	
	Mg^{2+}	Mn^{2+}
	pmol UMP incorporated/min/μg	
Wild type	10	90
D238A	0.8	40
D238E	0.4	40
D238F	0.2	4
D238N	0.1	40
D238V	0.4	10
N297A	8	80
N297D	6	80
N297Q	2	30
N297V	4	50

[a] Specific activity values reported have been rounded to one significant figure.

Activity on sym/sub—While evaluation of poly(rU) polymerase activity and related activities of 3D^{pol} derivatives is useful

TABLE III
Kinetics of AMP incorporation into sym/sub catalyzed by wild-type 3D^pol and 3D^pol derivatives

Rates were determined as described under "Experimental Procedures."

Enzyme	Rate		
	Mg^{2+}		Mn^{2+}, 100 μM ATP
	100 μM ATP	1000 μM ATP	
Wild type	17 ± 2	40 ± 5[a]	118 ± 12
D238A	0.040 ± 0.002	0.044 ± 0.003	2.3 ± 0.2
D238E	0.007 ± 0.001	0.013 ± 0.001	0.87 ± 0.02
D238F	<0.0001	<0.0001	
D238N	0.009 ± 0.001	0.015 ± 0.002	0.94 ± 0.05
D238V	<0.0001	<0.0001	
N297A	1.9 ± 0.4	3.4 ± 0.2	5.4 ± 0.6
N297D	6.5 ± 0.8	16.3 ± 1.2	25 ± 5
N297Q	0.25 ± 0.01	0.59 ± 0.02	0.84 ± 0.13
N297V	2.6 ± 0.2	7.3 ± 0.6	5.8 ± 1.1

[a] The 2-fold difference in wild-type $3D^{pol}$ activity compared with Table IV is due to the increased ionic strength of these enzyme preparations compared with those purified by using the complete protein purification procedure.

as a first step, the fact that the rate-limiting step for this reaction reflects template switching limits the utility of the resulting data (19). We recently reported the development of a symmetrical primer-template substrate (sym/sub) suitable for evaluation of the kinetics and mechanism of $3D^{pol}$-catalyzed RNA synthesis (48). We have used this system to characterize further each $3D^{pol}$ derivative. The kinetics of AMP incorporation were evaluated for each $3D^{pol}$ derivative at two concentrations of ATP: 100 and 1000 μM. The K_d value of wild-type $3D^{pol}$ for ATP is approximately 100 μM.[2]

The position 238 derivatives had the following order of activity: D238A > D238E = D238N > D238F/D238V (Table III). The D238A derivative was 400–900-fold less active than the wild-type enzyme. This reduction in activity could not be attributed to defects in nucleotide binding for this derivative (or any other), because a 10-fold increase in ATP concentration never produced more than a 2-fold increase in the observed rate of AMP incorporation.

The position 297 derivatives had the following order of activity: N297D > N297V > N297A > N297Q (Table III), representing a 2–70-fold reduction in activity relative to wild-type $3D^{pol}$. This range of activity relative to wild-type $3D^{pol}$ is significantly different from the 2–5-fold decrease in activity observed by using the poly(rU) polymerase assay. This difference probably reflects a change in the rate-limiting step measured by the different assays: template switching (poly(rU) polymerase assay) (19) and elongation (sym/sub assay) (48).

The rates of single nucleotide incorporation were also determined by using Mn^{2+} as the divalent cation cofactor at a single concentration of ATP (100 μM). Mn^{2+} also stimulated AMP incorporation into sym/sub for each derivative analyzed. The relative order of activity of both position 238 and 297 derivatives was consistent with that observed in Mg^{2+}. However, differences existed between the extent of Mn^{2+} rescue observed by using the sym/sub assay relative to that observed by using the poly(rU) polymerase assay. By employing preassembled $3D^{pol}$-sym/sub complexes and an EDTA quench, the effect of Mn^{2+} reflects the increased stability of the $3D^{pol}$-sym/sub-ATP complex that undergoes catalysis.[3] In contrast, by employing dT_{15}/rA_{30}, the effect of Mn^{2+} reflects both an increase in the observed rate of nucleotide incorporation due to a more stable ternary complex and a decrease in the K_m value for $3D^{pol}$ binding to dT_{15}/rA_{30} (19, 20).

By using sym/sub it is possible to determine the kinetic parameters, k_{pol} and K_d, for nucleotide incorporation and calculate the specificity constant, k_{pol}/K_d. This analysis permits a more direct evaluation of the role of these residues in nucleotide selection. Two derivatives were selected for analysis: D238A and N297A. For this analysis, these two derivatives were purified by using the complete purification procedure (55).

The wild-type enzyme utilizes AMP 216-fold better than dAMP (Table IV). The selection by the enzyme for the rNTP occurs primarily during incorporation (108-fold) rather than binding (2-fold) (Table IV). The D238A derivative was incapable of distinguishing ATP from dATP (Table IV). The k_{pol} value of this enzyme for both nucleotides was decreased 2000-fold relative to wild-type $3D^{pol}$. This difference may reflect a change in the rate-limiting step for this derivative; perhaps the chemical step is now the rate-limiting step for incorporation. If the rate of the chemical step is decreased, then the apparent reduction in the K_d value for nucleotides may reflect the constant for a different species (intermediate) in the reaction pathway rather than an increase in the affinity of the enzyme for nucleotide (35).

These data are consistent with observations made by Joyce and colleagues with Klenow fragment (26–28). Mutation of Glu-710 in this enzyme to alanine resulted in an enzyme capable of incorporating rNTPs (27, 28). However, the maximal rate of dNMP incorporation was dramatically reduced relative to wild-type enzyme, suggesting a more direct role for this residue in phosphoryl transfer (27, 28).

In contrast to the complex phenotype of the D238A derivative, the phenotype of the N297A derivative is more easily interpreted. The role of Asn-297 in 2′-OH selection is probably very similar to that predicted for His-784 in T7 RNA polymerase (*i.e.* to provide a direct hydrogen bond (46)). The N297A derivative had a 10-fold reduction in the ability to distinguish rNTPs from 2′-dNTPs (Table IV). This reduction in specificity is due to a decrease in the efficiency of rNTP incorporation rather than a decrease in the affinity of the enzyme for rNTPs (Table IV). It is possible that an interaction between Asn-297 and the 2′-OH of the rNTP, as indicated in the structural model (Fig. 2*B*), stabilizes the catalytically competent ternary complex. If this complex "opens" more frequently in the absence of this interaction, then the observed rate of incorporation would be reduced. A similar argument can be used to explain the reduced rate of dNMP incorporation relative to ribonucleoside monophosphate incorporation for the wild-type enzyme (Table IV). The finding that the N297A derivative is only 10-fold slower than the wild-type enzyme instead of 100-fold suggests that an additional residue may interact with the 2′-OH of the incoming rNTP. It is possible that another residue (*e.g.* Asp-238) has this function (1).

Model for Ribonucleotide Selection by 3D^pol—In Fig. 2*D*, we present our working hypothesis for the mechanism of rNTP selection by $3D^{pol}$. Upon binding of an rNTP to the nucleotide-binding pocket, there may be a conformational change that positions Asp-238 and Asn-297 within hydrogen-bonding distance of the 2′-OH and positions the backbone amide of Asp-238 within hydrogen-bonding distance of the 3′-OH. A stable conformation of the 3′-OH may be required for hydrogen bonding to an oxygen of the β-phosphate, which, in turn, may facilitate phosphoryl transfer by restricting the mobility of the tripolyphosphate. The position of the Asp-238 side chain may be fixed by interactions with the side chain of Thr-293 and the backbone amide of Ser-288.

Is there a hydrogen bond between Asp-238 and Asn-297? The data presented herein are not sufficient to completely rule out

[2] J. J. Arnold and C. E. Cameron, manuscript in preparation.
[3] J. J. Arnold, D. W. Gohara, and C. E. Cameron, manuscript in preparation.

TABLE IV
Kinetic parameters for AMP and dAMP incorporation into sym/sub by wild-type 3D^{pol} and 3D^{pol} derivatives at 30 °C
Parameters were determined as described under "Experimental Procedures."

Enzyme	Nucleotide substrate						
	ATP			dATP			
	k_{pol}	K_d	k_{pol}/K_d	k_{pol}	K_d	k_{pol}/K_d	$(k_{pol}/K_d)_{ATP}/(k_{pol}/K_d)_{dATP}$
	s^{-1}	μM	$\mu M^{-1}s^{-1}$	s^{-1}	μM	$\mu M^{-1}s^{-1}$	
WT[a]	86.7 ± 3.7	133 ± 18	0.65 ± 0.09	0.80 ± 0.06	284 ± 59	0.0030 ± 0.0006	216
D238A	0.044 ± 0.002	41 ± 5	0.0010 ± 0.0001	0.037 ± 0.001	30 ± 2	0.0010 ± 0.0001	1
N297A	4.6 ± 0.2	176 ± 31	0.030 ± 0.005	0.22 ± 0.03	256 ± 29	0.0010 ± 0.0004	30

[a] Values taken from J. J. Arnold and C. E. Cameron (manuscript in preparation).

this possibility. However, for the following reasons, we have not included this interaction in the model shown in Fig. 2*D*. First, it was not possible to orient the carboxamide of Asn-297 such that it interacted with both the 2′-OH of the rNTP and the carboxylate of Asn-238. Second, our data showed that Asn-297 was not essential for positioning Asp-238 (based upon the lack of equivalence of the phenotypes for N297A and D238A) but was required for interactions with the 2′-OH (Table IV). More rigorous analysis of the alanine derivatives, including kinetic analysis of the two derivatives with nucleotide analogs, is in progress to clarify this issue.

We added the additional interactions shown in Fig. 2*D* to explain the biochemical data reported in Tables II–IV. In the absence of Asn-297, Asp-238 remains in place, presumably due to other interactions in the pocket. Clearly, Thr-293 and Ser-288 are in a position to function in this capacity. D238A is impaired in its ability not only to select for rNTPs but also to catalyze phosphoryl transfer. The ability of this side chain to communicate with the active site, a distance of 10 Å, can be explained by the model as follows. The conformation of the tripolyphosphate requires a stable conformation of the 3′-OH, which is dependent upon the position of the Asp-238 backbone, and the position of the backbone is dependent upon the conformation of the Asp-238 side chain. Such an intricate network of hydrogen bonds should be capable of communicating to the active site that a nucleotide with the incorrect sugar configuration has been bound. In addition, given the close packing within the pocket, binding of nucleotides with an incorrect base may also be communicated to the active site by perturbing the position of Asp-238.

Activity In Vivo—The poly(rU) polymerase assay showed that the N297A, N297D, and N297Q derivatives retained 80, 60, and 20% of the wild-type activity, respectively. If these values reflect the biological activity, then it is reasonable to predict that the N297A and N297D derivatives might support virus multiplication, while the N297Q might exhibit a delayed growth phenotype or not support any virus growth. In contrast, the sym/sub assay showed that the N297A, N297D, and N297Q derivatives retained 10, 40, and 1% of the wild-type activity, respectively. Based upon these data, it is reasonable to predict that virus containing a 3D^{pol}-N297D substitution might be viable, but a virus containing 3D^{pol}-N297A or 3D^{pol}-N297Q might not. A series of poliovirus variants were constructed containing these specific alterations in 3D^{pol} to determine which of the two *in vitro* polymerase assays is more relevant biologically.

The viability of the mutant polioviruses was determined by high efficiency transfection with *in vitro* transcribed viral RNA. A productive infection was established in 4.3% (5×10^4) of the transfected cells by using wild-type poliovirus RNA or the MoΔNde1 variant at 37 °C (Table V), as scored in an infectious center assay (see "Experimental Procedures"). MoΔNde1-3D^{pol}238A, MoΔNde1-3D^{pol}297A, MoΔNde1-3D^{pol}297D, and MoΔNde1-3D^{pol}297Q were all inviable at 37 °C (Table V).

TABLE V
Biological analysis of poliovirus mutants

Virus	37 °C	32 °C
	pfu[a]/transfection[b]	*pfu*/*transfection*[c]
Mo	5×10^4	5×10^4
MoΔNde1	5×10^4	5×10^4
MoΔNde1–3D^{pol}D238A	0[d]	0[d]
MoΔNde1–3D^{pol}N297A	0	0
MoΔNde1–3D^{pol}N297D	0[e]	2×10^4
MoΔNde1–3D^{pol}N297Q	0	0

[a] pfu, plaque-forming units.
[b] 37 °C plaque assays were observed for up to 7 days post-transfection. Wild-type virus was scored on day 2.
[c] 32 °C plaque assays were observed for up to 8 days post-transfection. Wild-type virus was scored on day 3.
[d] Rare (2/transfection) plaques were recovered. These viruses were sequenced to confirm that they had reverted from 238A (codon GCT) to the wild-type 238D (codon GAT), and still possessed the MoΔNde1 silent marker mutations. The single point mutations were most likely generated during the *in vitro* transcription reactions.
[e] Rare (~10/transfection) plaques were recovered. By plaque appearance, these viruses fell into two classes: wild-type revertants (1–3 wild-type size plaques/transfection) and second site suppressor mutants (8–10 small plaques/transfection).

Transfections were repeated at 32 °C and showed that only MoΔNde1-3D^{pol}297D was viable (Table V). Interestingly, MoΔNde1-3D^{pol}297D was temperature-sensitive and only formed small plaques at 6 days after transfection, 4 days slower than wild-type virus (Fig. 3*A*).

To determine more directly the effect of these substitutions on RNA synthesis, a poliovirus replicon (polioLuc) that consists of a full-length poliovirus genome with the capsid genes replaced by a luciferase reporter gene was employed (Fig. 3*B*). Upon transfection into HeLa cells, polioLuc translates and replicates at levels comparable with wild-type poliovirus (58). A representative set of 3D^{pol} mutations were subcloned into the replicon plasmid, and translation and replication of the corresponding RNAs were evaluated at 37 and 32 °C (Fig. 3, *C* and *D*). Poliovirus replication is inhibited by 2 mM guanidine. Therefore, luciferase activity obtained from polioLuc transfection in the presence of 2 mM guanidine is a measure of the translation of the input RNA. RNA for all derivatives was translated at wild-type levels. As expected, polioLuc-3D^{pol}238A completely failed to replicate. PolioLuc-3D^{pol}297A replicated to levels slightly above background at both 37 and 32 °C, demonstrating a serious defect for replication *in vivo*. PolioLuc-3D^{pol}297D clearly replicated both at 32 and 37 °C but was 10-fold lower than wild-type replication levels at its peak at 37 °C, whereas 50% of the wild-type replication level was observed at 11 h after transfection at 32 °C (Fig. 3, *C* and *D*).

Taken together, these data demonstrate a direct correlation between the kinetics of elongation on sym/sub *in vitro* and the kinetics of RNA synthesis *in vivo*. These results support the hypothesis that sym/sub recapitulates the biologically relevant elongation reaction. A 2.5-fold reduction in the elongation rate of 3D^{pol} confers a temperature-sensitive growth phenotype on

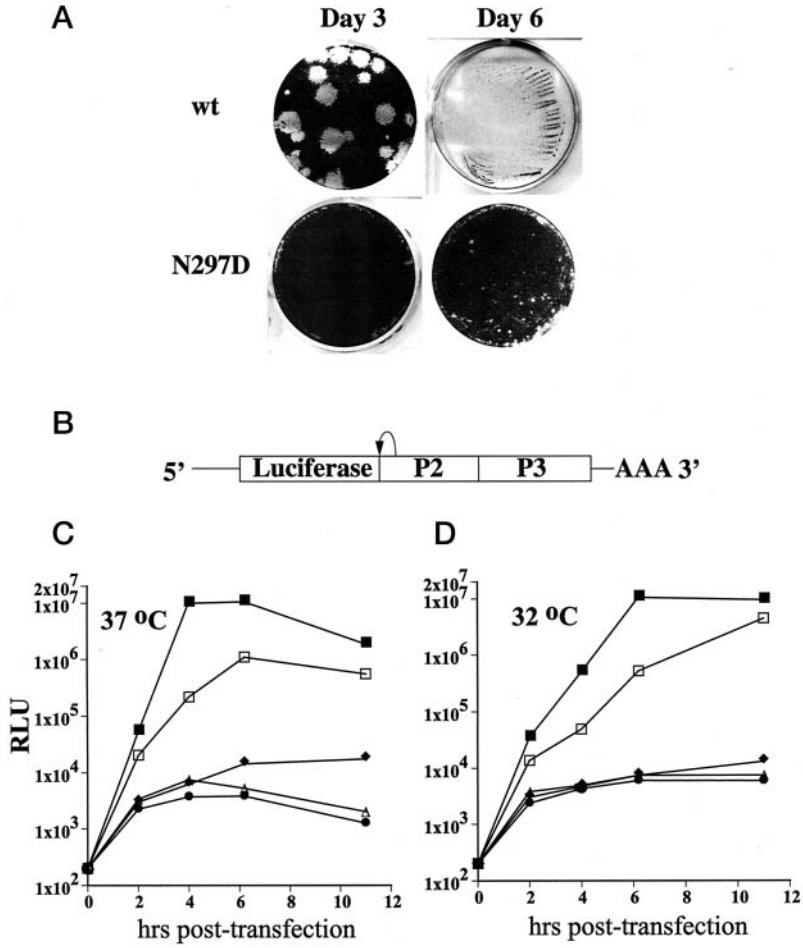

FIG. 3. **Biological analysis of 3D^{pol} variants.** *A*, infectious center assay. HeLa cells were transfected with viral RNA (MoΔNde1 or MoΔNde1-3D^{pol}297D) and then serially diluted and plated on a monolayer of untransfected HeLa cells. Plates were overlaid with an agar/medium agar medium (no 1) (see "Experimental Procedures") and incubated at 32 °C. Plates were developed on day 3 or day 6 after transfection. Plates containing transfected cells plated at a 1000-fold dilution are shown. Pinpoint plaques are visible on the MoΔNde1-3D^{pol}297D plate by day 6, when a comparable Mo-transfected plate has been completely lysed. Plaque assays were repeated numerous times. *B*, schematic diagram of polioLuc. PolioLuc is a poliovirus replicon that consists of a full-length poliovirus genome with the capsid genes replaced by a luciferase reporter gene. Upon translation, the active luciferase protein is cleaved away from the viral polyprotein by the viral protease 2A. *C*, PolioLuc replicons at 37 °C. This experiment was performed in triplicate, and a representative experiment is shown. ■, wild-type polioLuc; ●, wild-type polioLuc plus 2 mM guanidine; △, polioLuc-3D^{pol}238A; ♦, polioLuc-3D^{pol}297A; □, polioLuc-3D^{pol}297D. *D*, PolioLuc replicons at 32 °C. Experiment was performed in triplicate, and a representative experiment is shown. *Symbols* are as in *C*.

the virus. Changes at position 297 should affect nucleotide selection and may also change the overall fidelity of this derivative relative to wild-type 3D^{pol}. Therefore, additional studies with other derivatives will be necessary to prove that the biological phenotype associated with the virus containing the N297D substitution in 3D^{pol} is due solely to a defect in the rate of elongation. Nevertheless, it is reasonable to conclude that complete inhibition of viral RNA transcription and replication is not necessary to reduce significantly virus production. Although the molecular basis for this observation remains to be determined, it is intriguing to speculate that the observed synergy is related to the kinetic coupling of RNA synthesis and downstream processes such as packaging (66).

Acknowledgments—We thank Dr. Greg Farber for providing access to graphics workstations, Dr. Hemant Yennawar for expert technical assistance in various aspects of model construction, and Dr. Stephen Harrison for providing access to coordinates prior to publication.

REFERENCES

1. Hansen, J. L., Long, A. M., and Schultz, S. C. (1997) *Structure* **5,** 1109–1122
2. Ollis, D. L., Kline, C., and Steitz, T. A. (1985) *Nature* **313,** 818–819
3. Eick, D., Wedel, A., and Heumann, H. (1994) *Trends Genet.* 292–296
4. Hermann, T., Meier, T., Gotte, M., and Heumann, H. (1994) *Nucleic Acids Res.* **22,** 4625–4633
5. Doublie, S., Tabor, S., Long, A. M., Richardson, C. C., and Ellenberger, T. (1998) *Nature* **391,** 251–258
6. Kiefer, J. R., Mao, C., Braman, J. C., and Beese, L. S. (1998) *Nature* **391,** 304–307
7. Huang, H., Chopra, R., Verdine, G. L., and Harrison, S. C. (1998) *Science* **282,** 1669–1675
8. Doublie, S., and Ellenberger, T. (1998) *Curr. Opin. Struct. Biol.* **8,** 704–712
9. Boyer, P. L., Ferris, A. L., Clark, P., Whitmer, J., Frank, P., Tantillo, C., Arnold, E., and Hughes, S. H. (1994) *J. Mol. Biol.* **243,** 472–483
10. Ago, H., Adachi, T., Yoshida, A., Yamamoto, M., Habuka, N., Yatsunami, K., and Miyano, M. (1999) *Struct. Fold. Des.* **7,** 1417–1426
11. Lesburg, C. A., Cable, M. B., Ferrari, E., Hong, Z., Mannarino, A. F., and Weber, P. C. (1999) *Nat. Struct. Biol.* **6,** 937–943
12. Steitz, T. A., and Steitz, J. A. (1993) *Proc. Natl. Acad. Sci. U. S. A.* **90,** 6498–6502
13. Steitz, T. A. (1999) *J. Biol. Chem.* **274,** 17395–17398
14. Kuchta, R. D., Mizrahi, V., Benkovic, P. A., Johnson, K. A., and Benkovic, S. J. (1987) *Biochemistry* **26,** 8410–8417
15. Patel, S. S., Wong, I., and Johnson, K. A. (1991) *Biochemistry* **30,** 511–525
16. Reardon, J. E. (1993) *J. Biol. Chem.* **268,** 8743–8751
17. Jia, Y., and Patel, S. S. (1997) *J. Biol. Chem.* **272,** 30147–30153
18. Benkovic, S. J., and Cameron, C. E. (1995) *Methods Enzymol.* **262,** 257–269
19. Arnold, J. J., and Cameron, C. E. (1999) *J. Biol. Chem.* **274,** 2706–2716
20. Arnold, J. J., Ghosh, S. K., and Cameron, C. E. (1999) *J. Biol. Chem.* **274,** 37060–37069
21. Ricchetti, M., and Buc, H. (1993) *EMBO J.* **12,** 387–396
22. Arnaud-Barbe, N., Cheynet-Sauvion, V., Oriol, G., Mandrand, B., and Mallet, F. (1998) *Nucleic Acids Res.* **26,** 3550–3554
23. Joyce, C. M. (1997) *Proc. Natl. Acad. Sci. U. S. A.* **94,** 1619–1622
24. Kornberg, A., and Baker, T. (1991) *DNA Replication*, 2nd Ed., W. H. Freeman and Co., New York
25. Huang, Y., Eckstein, F., Padilla, R., and Sousa, R. (1997) *Biochemistry* **36,** 8231–8242
26. Minnick, D. T., Astatke, M., Joyce, C. M., and Kunkel, T. A. (1996) *J. Biol. Chem.* **271,** 24954–24961
27. Astatke, M., Grindley, N. D., and Joyce, C. M. (1998) *J. Mol. Biol.* **278,** 147–165
28. Astatke, M., Ng, K., Grindley, N. D., and Joyce, C. M. (1998) *Proc. Natl. Acad. Sci. U. S. A.* **95,** 3402–3407
29. Zinnen, S., Hsieh, J. C., and Modrich, P. (1994) *J. Biol. Chem.* **269,** 24195–24202
30. Gao, G., Orlova, M., Georgiadis, M. M., Hendrickson, W. A., and Goff, S. P. (1997) *Proc. Natl. Acad. Sci. U. S. A.* **94,** 407–411
31. Rienitz, A., Grosse, F., Blocker, H., Frank, R., and Krauss, G. (1985) *Nucleic Acids Res.* **13,** 5685–5695
32. Tabor, S., and Richardson, C. C. (1989) *Proc. Natl. Acad. Sci. U. S. A.* **86,** 4076–4080
33. Beard, W. A., Minnick, D. T., Wade, C. L., Prasad, R., Won, R. L., Kumar, A., Kunkel, T. A., and Wilson, S. H. (1996) *J. Biol. Chem.* **271,** 12213–12220
34. Astatke, M. Grindley, N. D. F., and Joyce, C. M. (1995) *J. Biol. Chem.* **270,** 1945–1954
35. Spence, R. A., Kati, W. M., Anderson, K. S., and Johnson, K. A. (1995) *Science* **267,** 988–993
36. Brandis, J. W., Edwards, S. G., and Johnson, K. A. (1996) *Biochemistry* **35,** 2189–2200
37. Lewis, D. A., Bebenek, K., Beard, W. A., Wilson, S. H., and Kunkel, T. A. (1999) *J. Biol. Chem.* **274,** 32924–32930
38. Boyer, P. L., Sarafianos, S. G., Arnold, E., and Hughes, S. H. (2000) *Proc. Natl.*

Acad. Sci. U. S. A. **97,** 3056–3061
39. Kaushik, N., Singh, K., Alluru, I., and Modak, M. J. (1999) *Biochemistry* **38,** 2617–2627
40. Bonnin, A., Lazaro, J. M., Blanco, L., and Salas, M. (1999) *J. Mol. Biol.* **290,** 241–251
41. Harris, D., Kaushik, N., Pandey, P. K., Yadav, P. N., and Pandey, V. N. (1998) *J. Biol. Chem.* **273,** 33624–33634
42. Kaushik, N., Harris, D., Rege, N., Modak, M. J., Yadav, P. N., and Pandey, V. N. (1997) *Biochemistry* **36,** 14430–14438
43. Gutierrez-Rivas, M., Ibanez, A., Martinez, M. A., Domingo, E., and Menendez-Arias, L. (1999) *J. Mol. Biol.* **290,** 615–625
44. Brieba, L. G., and Sousa, R. (2000) *Biochemistry* **39,** 919–923
45. Cheetham, G. M., Jeruzalmi, D., and Steitz, T. A. (1999) *Nature* **399,** 80–83
46. Cheetham, G. M., and Steitz, T. A. (1999) *Science* **286,** 2305–2309
47. Rechinsky, V. O., Kostyuk, D. A., Tunitskaya, V. L., and Kochetkov, S. N. (1992) *FEBS Lett.* **306,** 129–132
48. Arnold, J. J., and Cameron, C. E. (2000) *J. Biol. Chem.* **275,** 5329–5336
49. Bailey, S. (1994) *Acta Crystallogr. Sec. D Biol. Crystallogr.* **50,** 760–763
50. Jones, T. A., Zhou, J.-Y., Cowan, S. W., and Kjeldgaard M. (1991) *Acta Crystallogr. Sec. D Biol. Crystallogr.* **47,** 110–119
51. Brunger, A. T. (1998) *Acta Crystallogr. Sec. D Biol. Crystallogr.* **54,** 905–921
52. Berendsen, R. (1984) *J. Chem. Phys.* **81,** 3684–3690
53. Laskowski, R. A., McArthur, M. W., Moss, D. S., and Thornton, J. M. (1993) *J. Appl. Crystallogr.* **26,** 283–291
54. Aiyar, A., Xiang, Y., and Leis, J. (1996) *Methods Mol. Biol.* **57,** 177–191
55. Gohara, D. W., Ha, C. S., Ghosh, S. K. B., Arnold, J. J., Wisniewski, T. J., and Cameron, C. E. (1999) *Protein Expression Purif.* **17,** 128–138
56. Gill, S. C., and von Hippel, P. H. (1989) *Anal. Biochem.* **182,** 319–326
57. Johnson, K. A. (1986) *Methods Enzymol.* **134,** 677–705
58. Herold, A., and Andino, R. (2000) *J. Virol.*, **74,** 6394–6400
59. Andino, R., Rieckhof, G. E., Achacoso, P. L., Baltimore, D. (1993) *EMBO J.* **12,** 3587–3598
60. Crotty, S., Lohman, B. L., Lu, F. X., Tang, S., Miller. C. J., Andino, R. (1999) *J. Virol.* **73,** 9485–9495
61. Richards, O. C., Ehrenfeld, E. (1997) *J. Biol. Chem.* **272,** 23261–23264
62. Esteban, J. A., Salas, M., Blanco, L. (1993) *J. Biol. Chem.* **268,** 2719–2726
63. Koonin, E. V. (1991) *J. Gen. Virol.* **72,** 2197–2206
64. Lohmann, V., Korner, F., Herian, U., Bartenschlager, R. (1997) *J. Virol.* **71,** 8416–8428
65. Sankar, S., Porter, A. G. (1992) *J. Biol. Chem.* **267,** 10168–10176
66. Nugent, C. I., Johnson, K. L., Sarnow, P., Kirkegaard, K. (1999) *J. Virol.* **73,** 427–435
67. Fersht, A. (1999) *Structure and Mechanism in Protein Science: A Guide to Enzyme Catalysis and Protein Engineering*, p. 30, W. H. Freeman and Co., New York

Poliovirus RNA-dependent RNA Polymerase ($3D^{pol}$): STRUCTURAL, BIOCHEMICAL, AND BIOLOGICAL ANALYSIS OF CONSERVED STRUCTURAL MOTIFS A AND B

David W. Gohara, Shane Crotty, Jamie J. Arnold, Joshua D. Yoder, Raul Andino and Craig E. Cameron

J. Biol. Chem. 2000, 275:25523-25532.
doi: 10.1074/jbc.M002671200 originally published online May 25, 2000
